Published in final edited form as:
Biomech Model Mechanobiol. 2015 November ; 14(6): 1391–1402. doi:10.1007/s10237-015-0682-0.

Stress-mediated progression of solid tumors: effect of mechanical stress on tissue oxygenation, cancer cell proliferation and drug delivery

Fotios Mpekris, **Stelios Angeli**, **Athanassios P. Pirentis**, and **Triantafyllos Stylianopoulos***
Cancer Biophysics Laboratory, Department of Mechanical and Manufacturing Engineering, University of Cyprus, Nicosia, Cyprus

Abstract

Oxygen supply plays a central role in cancer cell proliferation. While vascular density increases at the early stages of carcinogenesis, mechanical solid stresses developed during growth compress tumor blood vessels and, thus, drastically reduce the supply of oxygen, but also the delivery of drugs at inner tumor regions. Among other effects, hypoxia and reduced drug delivery compromise the efficacy of radiation and chemo/nano therapy, respectively. In the present study, we developed a mathematical model of tumor growth to investigate the interconnections among tumor oxygenation that supports cancer cell proliferation, the heterogeneous accumulation of mechanical stresses owing to tumor growth, the non-uniform compression of intratumoral blood vessels due to the mechanical stresses, and the insufficient delivery of oxygen and therapeutic agents because of vessel compression. We found that the high vascular density and increased cancer cell proliferation often observed in the periphery compared to the interior of a tumor can be attributed to heterogeneous solid stress accumulation. Highly vascularized peripheral regions are also associated with greater oxygenation compared with the compressed, less vascularized inner regions. We also modeled the delivery of drugs of two distinct sizes, namely chemotherapy and nanomedicine. Model predictions suggest that drug delivery is affected negatively by vessel compression independently of the size of the therapeutic agent. Finally, we demonstrated the applicability of our model to actual geometries, employing a breast tumor model derived from MR images.

Keywords

mathematical modeling; hypoxia; vascular density; vessel collapse; tumor perfusion; nanomedicine; chemotherapy

1. Introduction

Sufficient tissue oxygenation is required for continuous proliferation of cancer cells. Accumulation of mechanical stresses within structural components of the tumor microenvironment, however, compresses intratumoral blood vessels reducing drastically

*Corresponding author: Cancer Biophysics Laboratory, Department of Mechanical and Manufacturing Engineering, University of Cyprus, P.O. Box 20537, Nicosia, 1678, Cyprus, tel: +357 2289.2238, fax: +357 2289.5081, tstylian@ucy.ac.cy.

Europe PMC Funders Author Manuscripts

oxygen supply and leading to hypoxia and necrosis (Griffon-Etienne et al. 1999; Padera et al. 2004; Stylianopoulos et al. 2012; Stylianopoulos et al. 2013). Furthermore, vessel compression reduces blood flow, which decreases the delivery of drugs compromising therapeutic outcomes (Chauhan et al. 2013; Jain 2013, 2014; Jain et al. 2014). Indeed, the growth of a tumor in the confined space of the host (normal) tissue results in the generation of external stresses exerted by the host tissue on the tumor, and the accumulation of internal solid stresses due to elastic interactions among tumor structural components (Skalak et al. 1996). Apart from compression of intratumoral vessels, that indirectly affects tumor growth through reduction in oxygen supply, these stresses are also exerted directly on cancer cells increasing their apoptotic rate and reducing their proliferation (Helmlinger et al. 1997; Kaufman et al. 2005; Cheng et al. 2009; Demou 2010; Tse et al. 2012; Desmaison et al. 2013; Delarue et al. 2014). In previous research, we estimated the growth-induced stresses, retained as “residual stresses”, to be in the range of 1.3-13.3 kPa (10 to 100 mmHg), high enough to collapse blood and lymphatic vessels (Stylianopoulos et al. 2012). We also found both experimentally and with the use of mathematical modeling that solid stresses are compressive at the interior of the tumor and tensile at the peripheral host tissue (Stylianopoulos et al. 2013). Consequently, the large amount of compressed vessels in the tumor often renders its interior hypo-vascular and hypo-perfused, which, in turn, should also cause non-uniform delivery of drugs to the tumor site and heterogeneous treatment.

The contribution of the mechanical microenvironment on tumor progression has been well recognized and biomechanical models of tumor growth have been developed to take into account the generation and accumulation of mechanical stresses in tumors (Ambrosi and Mollica 2002; Byrne and Preziosi 2003; Roose et al. 2003; Sarntinoranont et al. 2003; Kim et al. 2011; Ciarletta 2013; Ciarletta et al. 2013). Many of these models account for the direct effect of solid stress on cancer cell proliferation but the indirect effect of stress on vessel compression is not well studied (MacLaurin et al. 2012), and particularly its role in tumor progression and drug delivery. In the present study, we built on established modeling strategies, to develop a finite elements mathematical model that accounts for both direct and indirect effects of solid stress on tumor growth, as well as for the barriers posed by solid stress on the delivery and efficacy of chemo- and nano-therapies. Model predictions highlight the interdependence between oxygen supply, cancer cell proliferation, accumulation of solid stress, compression of blood vessels, reduction in vascular density and formation of hypoxia. Furthermore, we also studied how the concentration of drugs is hindered by solid stresses. We applied the model to two cases: the first case accounted for chemotherapy treatment and the second case accounted for a nanocarrier containing chemotherapy. Finally, our mathematical framework was implemented on an actual breast tumor model in order to assess its applicability to real geometries and its capability in addressing realistic tumor growth cases.

Europe PMC Funders Author Manuscripts

2. Materials and Methods

2.1 Description of the mathematical model

The mathematical model accounted for the growth of a spherical tumor surrounded by normal tissue. To describe the tumor's kinematics we used the multiplicative decomposition of the deformation gradient tensor

$$\mathbf{F}=\mathbf{F}_e\mathbf{F}_g. \quad (1)$$

In this fashion, the total deformation **F** of an infinitesimal material element is accounted for by local, non-stress generating volumetric growth ($\mathbf{F}_g$) with respect to the reference (stress-free) configuration, followed by an elastic deformation ($\mathbf{F}_e$) related to the stress response of the material that maintains continuity of the body and geometric compatibility between growing material elements (Rodriguez et al. 1994; Skalak et al. 1996; Ambrosi and Mollica 2002). The growth component $\mathbf{F}_g$ was set to be homogenous and isotropic (Roose et al. 2003; Kim et al. 2011; Stylianopoulos et al. 2013)

$$\mathbf{F}_g=\lambda_g\mathbf{I}, \quad (2)$$

where λ_g is the growth stretch ratio, which accounts for cancer cell proliferation. The elastic component $\mathbf{F}_e$ of the deformation gradient tensor is determined from Eq. (1) as

$$\mathbf{F}_e=\mathbf{F}\,\mathbf{F}_g^{-1}. \quad (3)$$

2.2 Calculation of growth stretch ratio λ_g

We calculated the growth rate of the tumor taking into account the oxygen concentration as well as the direct effect of solid stresses on reducing cancer cell proliferation in accordance with previous studies (Roose et al. 2003; Kim et al. 2011; MacLaurin et al. 2012; Voutouri and Stylianopoulos 2014). In particular, we used the expression

$$\frac{d\lambda_g}{dt}=\frac{1}{3}G\left(1+\beta\,\bar{\sigma}\right)S_f\,\Phi^c\,(1-\Phi^c)\,\lambda_g, \quad (4)$$

where $\bar{\sigma}=tr\boldsymbol{\sigma}^s/3=(\sigma_{rr}+\sigma_{\theta\theta}+\sigma_{\varphi\varphi})/3$ is the average (bulk) of the solid Cauchy stress $\boldsymbol{\sigma}^s$, β is a constant that describes the dependence of growth on solid stress and Φ^c is the volume fraction of the solid phase of the tumor. It was further assumed that only compressive solid stress inhibits tumor growth (Helmlinger et al. 1997; Cheng et al. 2009); therefore, we considered the term $(1+\beta\bar{\sigma})$ to be positive but less than unity when the bulk stress was compressive, and set it equal to unity when the bulk stress was tensile. The experimentally observed dependence of the volumetric growth rate on the local oxygen concentration is described by G and has the form (Casciari et al. 1992a,b)

$$G=\frac{k_1 c_{ox}}{k_2+c_{ox}}, \quad (5)$$

where k_1 and k_2 are growth rate parameters and c_{ox} is the oxygen concentration. Finally, to account for the effect of drug delivery on growth, the fraction of survived cells S_f is included in Eq. (4), so that in the absence of drugs S_f equals unity. The fraction of survived cells with respect to drug concentration has been previously measured experimentally for doxorubicin (Kerr et al. 1986), and the results were fitted to an exponential expression as a function of the internalized chemotherapy concentration c_{int}, i.e.,

$$S_f = exp\left(-\omega c_{int}\right), \quad (6)$$

where ω is a fitting parameter defined in (Eikenberry 2009).

2.3 Biphasic formulation of the tumor's mechanical behavior

The conservation of the tumor's solid and fluid phase is given by the following mass balance equations (Roose et al. 2003; Voutouri and Stylianopoulos 2014)

$$\frac{\partial \Phi^c}{\partial t} + \nabla \cdot \left(\Phi^c \mathbf{v}^s\right) = S^c, \quad (7)$$

$$\frac{\partial \Phi^f}{\partial t} + \nabla \cdot \left(\Phi^f \mathbf{v}^f\right) = Q, \quad (8)$$

where Φ^c and Φ^f are the volume fractions of the solid and fluid phases, respectively, and $\mathbf{v}^s$, $\mathbf{v}^f$ are the corresponding velocities. In the case of isotropic volumetric growth assumed herein, the growth stretch ratio and the creation/degradation rate of the solid phase S^c in the right hand side of Eq. (7) are related by (Ambrosi and Mollica 2002)

$$3\frac{1}{\lambda_g}\frac{d\lambda_g}{dt} = S^c. \quad (9)$$

In view of Eqs. (4) and (9), it follows that

$$S^c = G\left(1+\beta\,\bar{\sigma}\right) S_f\, \Phi^c\left(1-\Phi^c\right). \quad (10)$$

The term Q in the right hand side of Eq. (8) denotes the fluid flux entering from the blood vessels into the tumor or the surrounding normal tissue minus the fluid flux exiting through lymphatic vessels, and is expressed as (Stylianopoulos et al. 2013)

$$Q = L_p S_v\left(p_v - p_i\right) - L_{pl} S_{vl}\left(p_i - p_l\right), \quad (11)$$

where L_p, S_v and p_v are the hydraulic conductivity, vascular density and vascular pressure, respectively, L_{pl}, S_{vl} and p_l are the corresponding quantities for lymphatic vessels, and p_i is the interstitial fluid pressure. In our biphasic formulation, the sum of the solid and fluid volume fractions of tissue equals unity and it follows that

$$\Phi^f = 1 - \Phi^c. \quad (12)$$

Furthermore, summing Eqs. (7) and (8), the mass balance reads

$$\nabla \cdot \left(\Phi^c \mathbf{v}^s + \Phi^f \mathbf{v}^f \right) = Q + S^c, \quad (13)$$

where the fluid velocity $\mathbf{v}^f$ is given by Darcy's law (Byrne and Preziosi 2003)

$$\Phi^f \left(\mathbf{v}^f - \mathbf{v}^s \right) = - k_{th} \nabla p_i \quad \Rightarrow \quad \mathbf{v}^f = \frac{-k_{th} \nabla p_i}{\Phi^f} + \mathbf{v}^s, \quad (14)$$

with k_{th} the hydraulic conductivity of the interstitial space (Stylianopoulos et al. 2008).

According to the biphasic theory for soft tissues (Mow et al. 1980), the total stress tensor $\boldsymbol{\sigma}_{tot}$ is the sum of the fluid phase stress tensor $\boldsymbol{\sigma}^f = -p_i \mathbf{I}$ and the solid phase stress tensor $\boldsymbol{\sigma}^s$. As a result, the stress balance is written as

$$\nabla \cdot \boldsymbol{\sigma}_{tot} = \mathbf{0} \Rightarrow \nabla \cdot (\boldsymbol{\sigma}^{\mathbf{s}} - \mathbf{p_i I}) = \mathbf{0}, \quad (15)$$

where the Cauchy stress tensor of the solid phase $\boldsymbol{\sigma}^s$ is given by (Taber 2008)

$$\boldsymbol{\sigma}^s = J_e^{-1} \mathbf{F}_e \frac{\partial W}{\partial \mathbf{F}_e^T}. \quad (16)$$

The tumor mechanical behavior was modeled to be nearly-incompressible and described by the modified neo-Hookean strain energy density function (Xu et al. 2009,2010; Voutouri et al. 2014)

$$W = \frac{1}{2} \mu \left(-3 + II_1 \right) - p \left(J_e - 1 \right) - \frac{p^2}{2k}, \quad (17)$$

where μ and k are the shear and bulk modulus of the material, respectively, J_e is the determinant of the elastic deformation gradient tensor $\mathbf{F}_e$, $II_1 = I_1 J_e^{-2/3}$ where $I_1 = \mathrm{tr}\mathbf{C}_e$ is the first invariant of the elastic Cauchy-Green deformation tensor $\mathbf{C}_e = \mathbf{F}_e^{\mathrm{T}} \mathbf{F}_e$, p is a Lagrange multiplier enforcing the material constraint and the third term on the right hand side of Eq. (17) is a penalty term introduced for nearly incompressible materials that regularizes the constraint involved in the second term (Holzapfel 2000). The surrounding normal tissue was assumed to be compressible and neo-Hookean with a Poisson ratio of 0.2. Values for all parameters above are provided in Table 1 and Supplementary Table 1.

2.4 Vascular density

To quantify the vascular density we consider that it is affected independently both by solid stress and angiogenesis. To incorporate the effect of the former, we considered the vascular density as the vascular surface area S per unit volume, with S given by

$$S = \pi d L N, \quad (18)$$

where d, L and N are the diameter, length and number of vessels, respectively. Assuming that solid stress does not affect the number or length of vessels, but only their diameter, the change in vascular density due to vessel compression is expressed as

$$S_V\left(\bar{\sigma}\right) = (d/d_0)\ S_{V0}, \quad (19)$$

where S_{V0} and d_0 are the vascular density and vessel diameter values when no compression is applied. The changes of the ratio d/d_0 were determined as follows. We performed simulations in which we modeled a tumor blood vessel with a length of 100 μm and diameter of 30 μm embedded in a solid tumor (Supplementary Fig. 1a). We increased the uniform stress exerted on the vessel wall and calculated the relative decrease in the diameter of the vessel (Supplementary Fig. 1b). The vessel wall was assumed to be neo-Hookean, with the same material properties as the normal tissue, given in Table 1. When the stress of the solid matrix exceeded a critical value, the vessel became unstable and collapsed. We calculated the critical stress for the collapse of the tumor blood vessels to be −10.04 kPa, and fitted the results of the simulations to a second order polynomial function of the ratio d/d_0 (Supplementary Fig. 1b).

To incorporate the effect of angiogenesis, we assumed for our model the growth of a murine tumor, and set the initial vascular density of the host tissue to $S_{V0} = 70\ \text{cm}^{-1}$, whereas in the tumor S_{V0} was taken to follow a linear increase from 70 cm^{-1} at Day 0 to the value of 200 cm^{-1} at Day 10 (Baxter and Jain 1989; Stylianopoulos et al. 2013).

Finally, when the critical values of stress that caused vessel collapse were reached, it was further assumed that vascular density became zero within a period of two days.

2.5 Oxygen Concentration

The rate of change of oxygen in tissues depends on its transport through convection and diffusion, minus the amount of oxygen consumed by cells, plus the amount that enters the tissue from the blood vessels (Roose et al. 2003; Kim et al. 2011), i.e.,

$$\frac{\partial c_{ox}}{\partial t} + \nabla \cdot \left(c_{ox}\mathbf{v}^f\right) = D\nabla^2 c_{ox} - \frac{A_{ox}c_{ox}}{c_{ox}+k_{ox}} S_f \Phi^C + P_{er} S_V \left(C_{iox} - c_{ox}\right), \quad (20)$$

where c_{ox} is the oxygen concentration, D is the diffusion coefficient of oxygen in the interstitial space, A_{ox} and k_{ox} are oxygen uptake parameters, P_{er} is the vascular permeability of oxygen that describes diffusion across the tumor vessel wall and C_{iox} is the oxygen concentration in the vessels.

2.6 Drug transport

Delivery of chemotherapy—We assumed that chemotherapy affects the growth of the tumor by killing cancer cells but has no effect on endothelial cells and the tumor vascular density. The chemotherapeutic agent can exist in three distinct states: travel free in the interstitial space (c_f), bind to cancer cells (c_b), and internalized by cells (c_{int}). Hence, drug transport in the interstitial space is expressed as (Stylianopoulos and Jain 2013)

$$\begin{aligned}\frac{\partial c_f}{\partial t}+\nabla\cdot\left(c_f\mathbf{v}^f\right)&= D_f\nabla^2 c_f+Q_{sta}-\frac{k_{\mathrm{on}}c_e c_f}{\Phi}+k_{\mathrm{off}}c_b,\\ \frac{\partial c_b}{\partial t}+\nabla\cdot\left(c_b\mathbf{v}^s\right)&=\frac{k_{\mathrm{on}}c_e c_f}{\Phi}-k_{\mathrm{off}}c_b-k_{int}c_{int},\\ \frac{\partial c_{int}}{\partial t}+&\nabla\cdot\left(c_{int}\mathbf{v}^s\right)=k_{int}c_b,\end{aligned}\qquad(21)$$

where D_f is the diffusion coefficient of the drug in the tumor interstitial space, c_e is the concentration of cell surface receptors, k_{on}, k_{off} and k_{int} are the association (binding), dissociation and internalization rate constants of the drug with the cells, respectively, and Φ is the volume fraction of tumor accessible to the drug. The term Q_{sta} on the right hand side of Eq. $(21)_1$ denotes the transport of the drug across the tumor vessel wall and is given by Starling's approximation as (Stylianopoulos and Jain 2013)

$$Q_{sta}=P_{er}S_V\left(C_{iv}-c_f\right)+L_pS_V\left(P_V-p_i\right)\left(1-\sigma_f\right)C_{iv},\qquad(22)$$

where L_p is the hydraulic conductivity of the vessel wall, $C_{iv}=\exp(-(t-t_0)/k_d)$ is the vascular concentration of the drug, describing a bolus injection, with t_0 the time of drug injection and k_d the blood circulation decay, and σ_f is the reflection coefficient. The parameter L_p was calculated as a function of the vessel wall pore radius and the parameters P_{er} and σ_f as a function of the ratio of the drug radius to the radius of the pores of the vessel wall (Deen 1987). A detailed description of these calculations is given in the Supplementary Material.

Delivery of nanotherapy—In the case of the delivery of a nanoparticle carrier (c_n) containing the chemotherapy, the transport equations given in Eq. (21) are modified as

$$\begin{aligned}\frac{\partial c_n}{\partial t}+\nabla\cdot\left(c_n\mathbf{v}^f\right)&=D_n\nabla^2 c_n+Q_{sta}-k_{el}c_n,\\ \frac{\partial c_f}{\partial t}+\nabla\cdot\left(c_f\mathbf{v}^f\right)&= D_f\nabla^2 c_f+ak_{el}c_n-\frac{k_{\mathrm{on}}c_e c_f}{\Phi}+k_{\mathrm{off}}c_b,\\ \frac{\partial c_b}{\partial t}+\nabla\cdot\left(c_b\mathbf{v}^s\right)&=\frac{k_{\mathrm{on}}c_e c_f}{\Phi}-k_{\mathrm{off}}c_b-k_{int}c_{int},\\ \frac{\partial c_{int}}{\partial t}+&\nabla\cdot\left(c_{int}\mathbf{v}^s\right)=k_{int}c_b,\end{aligned}\qquad(23)$$

where k_{el} is the chemotherapy release rate constant and a is the number of chemotherapy molecules contained in the nanocarrier.

2.7 Solution strategy

The model consists of a spherical tumor domain with initial diameter of 500 μm, embedded at the center of a cubic host domain two orders of magnitude larger to avoid any boundary effects on the growth of the tumor; due to symmetry, only one eighth of the system was considered (Fig. 1). We simulated a murine tumor that grows within a period of 10 days. To this end, Eqs. (1)-(23) were solved simultaneously using the commercial finite element software COMSOL Multiphysics (COMSOL, Inc., Burlington, MA, USA). Values for the model parameters are provided in Table 1 and Supplementary Table 1. The boundary conditions employed are illustrated in Fig. 1. The boundary conditions for the continuity of the stress and displacement fields, as well as the concentration of the oxygen and the drug at the interface between the tumor and the normal tissue, were applied automatically by the software.

Europe PMC Funders Author Manuscripts

2.8 MRI based tumor model

For the extraction of the computational mesh of the human breast, a T2-Weighted stack of MR (Magnetic Resonance) images was imported in ScanIP (Simpleware Ltd, Exeter, UK). Subsequently, a thresholding operation was applied to allow the segmentation of the breast from the images, followed by cavity filling, island removal and Gaussian smoothing (sigma=1) to optimize the resulting mask. Finally, a second mask was manually created in a region centrally located, 35 mm behind the nipple, to act as the tumor in the simulation setup. The mesh was extracted using the FE Free algorithm of Simpleware and tetrahedral elements. The total number of finite elements comprising the model was 557,818 (Fig. 2). In terms of the solution strategy, the material properties and boundary conditions were taken to be the same as described previously, except from boundary conditions of the stress and displacement fields were no symmetry was exploited. Hence, the breast surface was allowed to move freely while the posterior part, which is adjacent to the chest cavity, was fixed.

3. Results

3.1 Magnitude of solid stress is higher at the tumor interior compared to the periphery

Growth-induced expansion of the tumor results in generation of stresses and displacement of the tumor and the surrounding host tissue (Supplementary Fig. 2). Solid stresses are compressive inside the tumor and spatially heterogeneous. Figure 3 depicts the circumferential (Fig. 3a) and radial (Fig. 3b) components of the solid stress at the center of tumor and at the periphery, as a function of time. The magnitude of the compressive stress is higher at the center compared to the periphery of the tumor resulting in heterogeneous stress distribution.

3.2 Heterogeneous stress distribution results in non-uniform tumor oxygenation and cancer cell proliferation

The heterogeneous distribution of solid stress observed in Fig. 3 will result in heterogeneous compression of blood vessels and, thus, heterogeneous vascular density inside the tumor. Figure 4a presents the spatial profile of vascular density at three time points. At the initial stages of tumor growth (Day 1), vascular density is uniform throughout the tumor and decreases from the interface to reach a normal baseline value inside the host tissue. Intratumoral vascular density increases with time owing to tumor-induced angiogenesis but as the tumor grows and solid stress is built up in the tissue, tumor vascular density becomes higher at the periphery compared to the interior of the tumor due to the compression of blood vessels (Day 4). When solid stress exceeds the critical value for vessel collapse, vascular density reduces to values less than that of the normal tissue baseline and the tumor interior becomes hypo-vascular (Day 7) in agreement with other models (Stoll et al. 2003).

Tumor oxygenation requires a sufficient vascular network. The spatial distribution of oxygen at different days presents a profile similar to that of the vascular density (Fig. 4b). Prior to vessel collapse, tumor tissue is well oxygenated but becomes hypoxic when blood vessels are blocked. These results suggest that hypoxia, a hallmark of tumor pathophysiology that regulates the expression of several biological factors (e.g., hypoxia inducible factors, vascular endothelial growth factors), can be attributed to the effect of

mechanical stress. Furthermore, larger oxygen concentrations and lower stresses at the tumor periphery gradually lead to higher values of cancer cell proliferation as suggested by the spatial profile of the proliferation stretch ratio λ_g (Fig. 4c), and in accordance with published experimental data (Cheng et al. 2009; Stylianopoulos et al. 2013).

3.3 Solid stress accumulation inhibits the delivery of drugs

To investigate the extent to which solid stress inhibits drug delivery, we modeled the intratumoral transport of two systems: (*i*) chemotherapy alone, and (*ii*) a nanoparticle delivery system where the chemotherapy was contained in a nanocarrier and was released in a controlled fashion. We modeled the drug administration as a bolus injection, performed either before (Day 3) or after (Day 6) vessel collapse, which took place on Day 5.1, when solid stress reaches the critical value. In the case of the chemotherapy, the size of the drug was taken to be 1 nm and the radius of the pores of the vessel wall varied from the normal value of 3.5 nm at Day 0 to the value of 120nm at Day 10, accounting for the increased permerability of tumor blood vessels (Hobbs et al. 1998). For the case of the nanoparticle, its size was 100 nm and to ensure its extravasation from the pores of the vessel wall simulations were performed for two pore sizes: 200 nm and 600 nm, respectively.

The spatial distribution of the drug concentration internalized by cancer cells when the drug was administered prior to vessel collapse is shown in Figs. 5a,b. For both drug delivery cases the concentration of the internalized drug is lower in the center of the tumor compared to the periphery. Inside the normal tissue the concentration of the drug for the case of chemotherapy alone is lower than in the tumor interior owing to the assumption of higher vascular density inside the tumor. In the case of nanotherapy, there is leakage of drug from the tumor to the surrounding normal tissue owing to the fluid pressure difference between the two tissues (Supplementary Fig. 3); however, the concentration of the drug becomes negligible away from the tumor because of selective extravasation of the nanocarrier through the leaky tumor vessels. When the drug is administered following vessel collapse (Figs. 5c,d) the concentration of the internalized drug decreases drastically, in accordance with experimental studies (Chauhan et al. 2013).

Figures 6a,b depict the temporal variation of the concentration of internalized drug administered prior to vessel collapse and of the fraction of survived cells, respectively, at the center of the tumor for chemotherapy and for nanotherapy. The first graph reveals the dependence of drug efficacy on the size of the delivery system. In particular, significantly less drug concentration is observed for nanotherapy with 200 nm pores compared to nanotherapy with 600 nm pores, or chemotherapy. On the other hand, in the second graph, more cells are observed to survive in the case of nanotherapy when the pores are 200 nm, due to smaller drug concentration. An increase in vessel wall pore size can significantly improve the delivery of nanocarriers and have a more profound effect on the fraction of cell survival.

3.4 Application of the mathematical framework in a real geometry of breast tumor

To test the applicability of the model to a real geometry, we implemented our mathematical framework to a breast tumor model based on MR images. Such an implementation

demonstrates the ability of the setup to produce accurate results without exploiting symmetries, while maintaining its stability in complex, irregular meshes with an increased number of degrees of freedom and actual material properties. As the tumor volume increases (Fig. 7a), the values of the displacements in the anterior and cranio-caudal directions of the breast become higher since these boundaries are free to deform (Fig. 7b). Similar to the simple geometry, stresses are compressive inside the tumor and tensile at the interface with the normal tissue (Fig.7c). Furthermore, the interstitial fluid pressure is uniform in the tumor interior and drops to normal tissue values at the periphery (Fig. 7d). Finally, as in the simple geometry, the breast tumor model predicts that the reduction of vascular density leads to hypoxia (Fig. 7e).

4. Discussion

The evolution of solid stresses has a strong impact on tumor growth. In the present study, we investigated the interplay between tumor oxygenation, cancer cell proliferation and accumulation of solid stresses and their effect on the delivery of therapeutic agents. Specifically, we showed that heterogeneous accumulation of stresses results in heterogeneous distribution of vascular density, with higher values at the periphery and lower at the center of the tumor. The hypo-vascular interior of the tumor results in hypoxia, which reduces cancer cell proliferation, and inefficient delivery of drugs, which affects the efficacy of the treatment. Our results highlight the importance of alleviation of these solid stresses with stress-alleviating agents in order to decompress blood vessels and improve tumor oxygenation, drug delivery and efficacy of chemotherapy. This stress alleviation strategy has been recently applied successfully in preclinical models and has been shown to improve the delivery of both chemotherapeutic agents and nanoparticles (Provenzano et al. 2012; Chauhan et al. 2013).

Several simplifying assumptions were made in the present study. In particular, vessel collapse was assumed to occur at the same critical stress value, and vascular pressure was taken to be the same throughout the tumor and unaffected by vessel compression. In a real situation, blood vessels do not collapse concurrently and vascular pressure depends on the structure of the vascular network, the degree of vessel compression as well as the permeability of the vessels and it decreases as we move from upstream to downstream vessels. Furthermore, vessel collapse is not equally observed in all tumor types and all tumors are not hypo-vascular. Tumors with abundant collapsed vessels are found in highly desmoplastic cancers, such as pancreatic and breast cancers and various sarcomas (Chauhan et al. 2013). However, vessel compression is a hallmark of tumor pathophysiology and should be observed in most tumor types (Padera et al. 2004; Stylianopoulos et al. 2013). Most of the model parameters were obtained from previous models and experimental data from literature; in the absence of data, some parameter values were chosen ad hoc. Despite this arbitrariness, the model predictions are reasonable, physiologically feasible and consistent with experimental observations, where available. Therefore, modifying any of the aforementioned assumptions would only alter the results quantitatively and it would not affect our general conclusions, in particular that heterogeneous accumulation of solid stress regulates tissue oxygenation, cancer cell proliferation and drug delivery.

Our mathematical approach is also subject to certain limitations. Specifically, the tumor was set to be near incompressible and proliferating in an isotropic fashion, which might not be true given the highly heterogeneous nature of solid tumors. On the other hand, the adoption of isotropic growth is a common approximation in literature, and we consider it sufficient for the purposes of the present study in the sense that it offers simplicity, mathematical transparency and it does not prevent the emergence of heterogeneous distributions and the agreement with experimental observations. Furthermore, the model can be easily modified to accommodate non-isotropic growth. In the model, vessel collapse resulted in a contemporary shut down of all intratumoral vessels at a certain instant. This can be considered a reasonable assumption for murine desmoplastic tumors in which the majority of blood vessels are rendered not functional from the early stages of carcinogenesis (Padera et al. 2004; Chauhan et al. 2013). In addition, the model does not account for vessel deformation in the extratumoral region. In the past, we have shown that peritumoral blood vessels do not collapse but deform to ellipsoid shapes (Stylianopoulos et al. 2013). For the sake of simplicity, the model also does not take into account the kinematic contribution of cell reorganization due to stress build-up. Such a contribution can be implemented by including an additional (plastic) part in the decomposition of the total deformation gradient tensor, corresponding to the rearrangement of cellular adhesion bonds without change of mass in the volume element (Ambrosi and Preziosi 2009; Giverso and Preziosi 2013). As most biological tissues, tumors have a complex and heterogeneous structure so that the use of the neo-Hookean constitutive equation might not be sufficient to fully describe their mechanical response. However, in previous research we showed that the state of stress of a tumor is largely determined by the properties of the host tissue and not from the constitutive equation that is used (Voutouri et al. 2014). Finally, we did not account for biological parameters affecting tumor progression, such as the role of vascular endothelial growth factor (VEGF) on tumor-induced angiogenesis or changes in the amount of collagen and other extracellular proteins owing to a desmoplastic response often observed in tumors, which would change the mechanical properties of the tissue during growth. Incorporation of these parameters is not expected to change our results qualitatively.

Supplementary Material

Refer to Web version on PubMed Central for supplementary material.

Acknowledgements

The research leading to these results has received funding from the European Research Council under the European Union's Seventh Framework Programme (FP7/2007-2013) / ERC grant agreement no 336839-ReEnginneeringCancer to TS. FM was partially supported by the University of Cyprus under the Programme "New Researchers".

References

Ambrosi D, Mollica F. On the mechanics of a growing tumor. Int J Eng Sci. 2002; 40:1297–1316.

Ambrosi D, Preziosi L. Cell adhesion mechanisms and stress relaxation in the mechanics of tumours. Biomech Model Mechanobiol. 2009; 8:397–413. [PubMed: 19115069]

Baxter LT, Jain RK. Transport of fluid and macromolecules in Tumors. I. Role of interstitial pressure and convection. Microvasc Res. 1989; 37:77–104. [PubMed: 2646512]

Byrne H, Preziosi L. Modelling solid tumour growth using the theory of mixtures. Math Med Biol. 2003; 20:341–366. [PubMed: 14969384]

Casciari JJ, Sotirchos SV, Sutherland RM. Variations in tumor-cell growth-rates and metabolism with oxygen concentration, glucose-concentration, and extracellular pH. J Cell Physiol. 1992a; 151:386–394. [PubMed: 1572910]

Casciari JJ, Sotirchos SV, Sutherland RM. Mathematical modeling of microenvironment and growth in EMT6/Ro multicellular tumor spheroids. Cell Proliferat. 1992b; 25:1–22. [PubMed: 1540680]

Chauhan VP, Stylianopoulos T, Martin JD, Popović Z, Chen O, Kamoun WS, Bawendi MG, Fukumura D, Jain RK. Normalization of tumour blood vessels improves the delivery of nanomedicines in a size-dependent manner. Nat Nanotechnol. 2012; 7:383–388. [PubMed: 22484912]

Chauhan VP, Martin JD, Liu H, Lacorre DA, Jain SR, Kozin SV, Stylianopoulos T, Mousa AS, Han X, Adstamongkonkul P, Popović Z, Huang P, Bawendi MG, Boucher Y, Jain RK. Angiotensin inhibition enhances drug delivery and potentiates chemotherapy by decompressing tumour blood vessels. Nat Commun. 2013; 4:2516. [PubMed: 24084631]

Cheng G, Tse J, Jain RK, Munn LL. Micro-environmental mechanical stress controls tumor spheroid size and morphology by suppressing proliferation and inducing apoptosis in cancer cells. Plos One. 2009; 4:e4632. [PubMed: 19247489]

Ciarletta P. Buckling instability in growing tumor spheroids. Phys Rev Lett. 2013; 110:158102. [PubMed: 25167314]

Ciarletta P, Ambrosi D, Maugin GA, Preziosi L. Mechano-transduction in tumour growth modelling. Eur Phys J E Soft Matter. 2013; 36:23. [PubMed: 23504484]

Dawidczyk CM, Kim C, Park JH, Russell LM, Lee KH, Pomper MG, Searson PC. State-of-the-art in design rules for drug delivery platforms: Lessons learned from FDA-approved nanomedicines. J Control Release. 2014; 187:133–144. [PubMed: 24874289]

Deen WM. Hindered transport of large molecules in liquid-filled pores. AIChE J. 1987; 33:1409–1425.

Delarue M, Montel F, Vignjevic D, Prost J, Joanny JF, Cappello G. Compressive stress inhibits porliferation in tumor spheroids through a volume limitation. Biophys J. 2014; 107:1821–1828. [PubMed: 25418163]

Demou ZN. Gene expression profiles in 3D tumor analogs indicate compressive strain differentially enhances metastatic potential. Ann Biomed Eng. 2010; 38:3509–3520. [PubMed: 20559731]

Desmaison A, Frongia C, Grenier K, Ducommun B, Lobjois V. Mechanical stress impairs mitosis progression in multi-cellular tumor spheroids. Plos One. 2013; 8:e80447. [PubMed: 24312473]

Eder M, Raith S, Jalali J, Volf A, Settles M, Machens HG, Kovacs L. Comparison of different material models to simulate 3-d breast deformations using finite element analysis. Ann Biomed Eng. 2014; 42:843–857. [PubMed: 24346816]

Eikenberry S. A tumor cord model for Doxorubicin delivery and dose optimization in solid tumors. Theor Biol Med Model. 2009; 6:16. [PubMed: 19664243]

Giverso C, Preziosi L. Behavior of cell aggregates under force-conrolled compression. Int J Nonlinear Mech. 2013; 56:50–55.

Griffon-Etienne G, Boucher Y, Brekken C, Suit HD, Jain RK. Taxane-induced apoptosis decompresses blood vessels and lowers interstitial fluid pressure in solid tumors: clinical implications. Cancer Res. 1999; 59:3776–3782. [PubMed: 10446995]

Helmlinger G, Netti PA, Lichtenbeld HC, Melder RJ, Jain RK. Solid stress inhibits the growth of multicellular tumor spheroids. Nat Biotechnol. 1997; 15:778–783. [PubMed: 9255794]

Hobbs SK, Monsky WL, Yuan F, Roberts WG, Griffith L, Torchilin VP, Jain RK. Regulation of transport pathways in tumor vessels: role of tumor type and microenvironment. Proc Natl Acad Sci USA. 1998; 95:4607–4612. [PubMed: 9539785]

Holzapfel. Nonlinear solid mechanics. Wiley; Chichester: 2000.

Jain RK. Normalizing tumor microenvironment to treat cancer: bench to bedside to biomarkers. J Clin Oncol. 2013; 31:2205–2218. [PubMed: 23669226]

Jain RK. An indirect way to tame cancer. Sci Am. 2014; 310:46–53. [PubMed: 24640331]

Jain RK, Martin JD, Stylianopoulos T. The role of mechanical forces in tumor growth and therapy. Annu Rev Biomed Eng. 2014; 16:321–346. [PubMed: 25014786]

Kaufman LJ, Brangwynne CP, Kasza KE, Filippidi E, Gordon VD, Deisboeck TS, Weitz DA. Glioma expansion in collagen I matrices: analyzing collagen concentration-dependent growth and motility patterns. Biophys J. 2005; 89:635–650. [PubMed: 15849239]

Kerr DJ, Kerr AM, Freshney RI, Kaye SB. Comparative intracellular uptake of adriamycin and 4′-deoxydoxorubicin by non-small cell lung-tumor cells in culture and its relationship to cell-survival. Biochem Pharmacol. 1986; 35:2817–2823. [PubMed: 3741470]

Kim Y, Stolarska MA, Othmer HG. The role of the microenvironment in tumor growth and invasion. Prog Biophys Mol Bio. 2011; 106:353–379. [PubMed: 21736894]

MacLaurin J, Chapman J, Jones GW, Roose T. The buckling of capillaries in solid tumours. P Roy Soc A-Math Phy. 2012; 468:4123–4145.

Mok W, Stylianopoulos T, Boucher Y, Jain RK. Mathematical modeling of herpes simplex virus distribution in solid tumors: implications for cancer gene therapy. Clin Cancer Res. 2009; 15:2352–2360. [PubMed: 19318482]

Mow VC, Kuei SC, Lai WM, Armstrong CG. Biphasic creep and stress-relaxation of articular-cartilage in compression - theory and experiments. J Biomech Eng-T ASME. 1980; 102:73–84. [PubMed: 7382457]

Netti PA, Berk DA, Swartz MA, Grodzinsky AJ, Jain RK. Role of extracellular matrix assembly in interstitial transport in solid tumors. Cancer Res. 2000; 60:2497–2503. [PubMed: 10811131]

Padera TP, Stoll BR, Tooredman JB, Capen D, di Tomaso E, Jain RK. Cancer cells compress intratumour vessels. Nature. 2004; 427:695–695. [PubMed: 14973470]

Pluen A, Bucher Y, Ramanujan S, McKee TD, Gohongi T, di Tomaso E, Brown EB, Izumi Y, Campbell RB, Berk DA, Jain RK. Role of tumor-host interactions in interstitial diffusion of macromolecules: cranial vs. subcutaneous tumors. Proc Natl Acad Sci USA. 2001; 98:4628–4633. [PubMed: 11274375]

Provenzano PP, Cuevas C, Chang AE, Goel VK, Von Hoff DD, Hingorani SR. Enzymatic targeting of the stroma ablates physical barriers to treatment of pancreatic ductal adenocarcinoma. Cancer Cell. 2012; 21:418–429. [PubMed: 22439937]

Rodriguez EK, Hoger A, McCulloch AD. Stress-dependent finite growth in soft elastic tissues. J Biomech. 1994; 27:455–467. [PubMed: 8188726]

Roose T, Netti PA, Munn LL, Boucher Y, Jain RK. Solid stress generated by spheroid growth estimated using a linear poroelasticity model. Microvasc Res. 2003; 66:204–212. [PubMed: 14609526]

Samani A, Zubovits J, Plewes D. Elastic moduli of normal and pathological human breast tissues: an inversion-technique-based investigation of 169 samples. Phys Med Biol. 2007; 52:1565–1576. [PubMed: 17327649]

Sarntinoranont M, Rooney F, Ferrari M. Interstitial stress and fluid pressure within a growing tumor. Ann Biomed Eng. 2003; 31:327–335. [PubMed: 12680730]

Schmidt MM, Wittrup KD. A modeling analysis of the effects of molecular size and binding affinity on tumor targeting. Mol Cancer Ther. 2009; 8:2861–2871. [PubMed: 19825804]

Skalak R, Zargaryan S, Jain RK, Netti PA, Hoger A. Compatibility and the genesis of residual stress by volumetric growth. J Math Biol. 1996; 34:889–914. [PubMed: 8858855]

Stoll BR, Migliorini C, Kadambi A, Munn LL, Jain RK. A mathematical model of the contribution of endothelial progenitor cells to angiogenesis in tumors: implications for antiangiogenic therapy. Blood. 2003; 102:2555–2561. [PubMed: 12775571]

Stylianopoulos T, Jain RK. Combining two strategies to improve perfusion and drug delivery in solid tumors. P Natl Acad Sci USA. 2013; 110:18632–18637. [PubMed: 24167277]

Stylianopoulos T, Martin JD, Chauhan VP, Jain SR, Diop-Frimpong B, Bardeesy N, Smith BL, Ferrone CR, Hornicek FJ, Boucher Y, Munn LL, Jain RK. Causes, consequences, and remedies for growth-induced solid stress in murine and human tumors. P Natl Acad Sci USA. 2012; 109:15101–15108. [PubMed: 22932871]

Stylianopoulos T, Martin JD, Snuderl M, Mpekris F, Jain SR, Jain RK. Coevolution of solid stress and interstitial fluid pressure in tumors during progression: implications for vascular collapse. Cancer Res. 2013; 73:3833–3841. [PubMed: 23633490]

Stylianopoulos T, Yeckel A, Derby JJ, Luo XJ, Shephard MS, Sander EA, Barocas VH. Permeability calculations in three-dimensional isotropic and oriented fiber networks. Phys Fluids. 2008; 20:123601. [PubMed: 19547721]

Taber LA. Theoretical study of Beloussov's hyper-restoration hypothesis for mechanical regulation of morphogenesis. Biomech Model Mechanobiol. 2008; 7:427–441. [PubMed: 17909868]

Tse JM, Cheng G, Tyrrell JA, Wilcox-Adelman SA, Boucher Y, Jain RK, Munn LL. Mechanical compression drives cancer cells toward invasive phenotype. Proc Natl Acad Sci U S A. 2012; 109:911–916. [PubMed: 22203958]

Wong C, Stylianopoulos T, Cui JA, Martin J, Chauhan VP, Jiang W, Popović Z, Jain RK, Bawendi MG, Fukumua D. Multistage nanoparticle delivery system for deep penetration into tumor tissue. P Natl Acad Sci USA. 2011; 108:2426–2431. [PubMed: 21245339]

Voutouri C, Mpekris F, Papageorgis P, Odysseos AD, Stylianopoulos T. Role of constitutive behavior and tumor-host mechanical interactions in the state of stress and growth of solid tumors. Plos One. 2014; 9:e104717. [PubMed: 25111061]

Voutouri C, Stylianopoulos T. Evolution of osmotic pressure in solid tumors. J Biomech. 2014; 47:3441–3447. [PubMed: 25287111]

Xu G, Bayly PV, Taber LA. Residual stress in the adult mouse brain. Biomech Model Mechanobiol. 2009; 8:253–262. [PubMed: 18651186]

Xu G, Kemp PS, Hwu JA, Beagley AM, Bayly PV, Taber LA. Opening angles and material properties of the early embryonic chick brain. J Biomech Eng. 2010; 132:011005. [PubMed: 20524743]

Europe PMC Funders Author Manuscripts

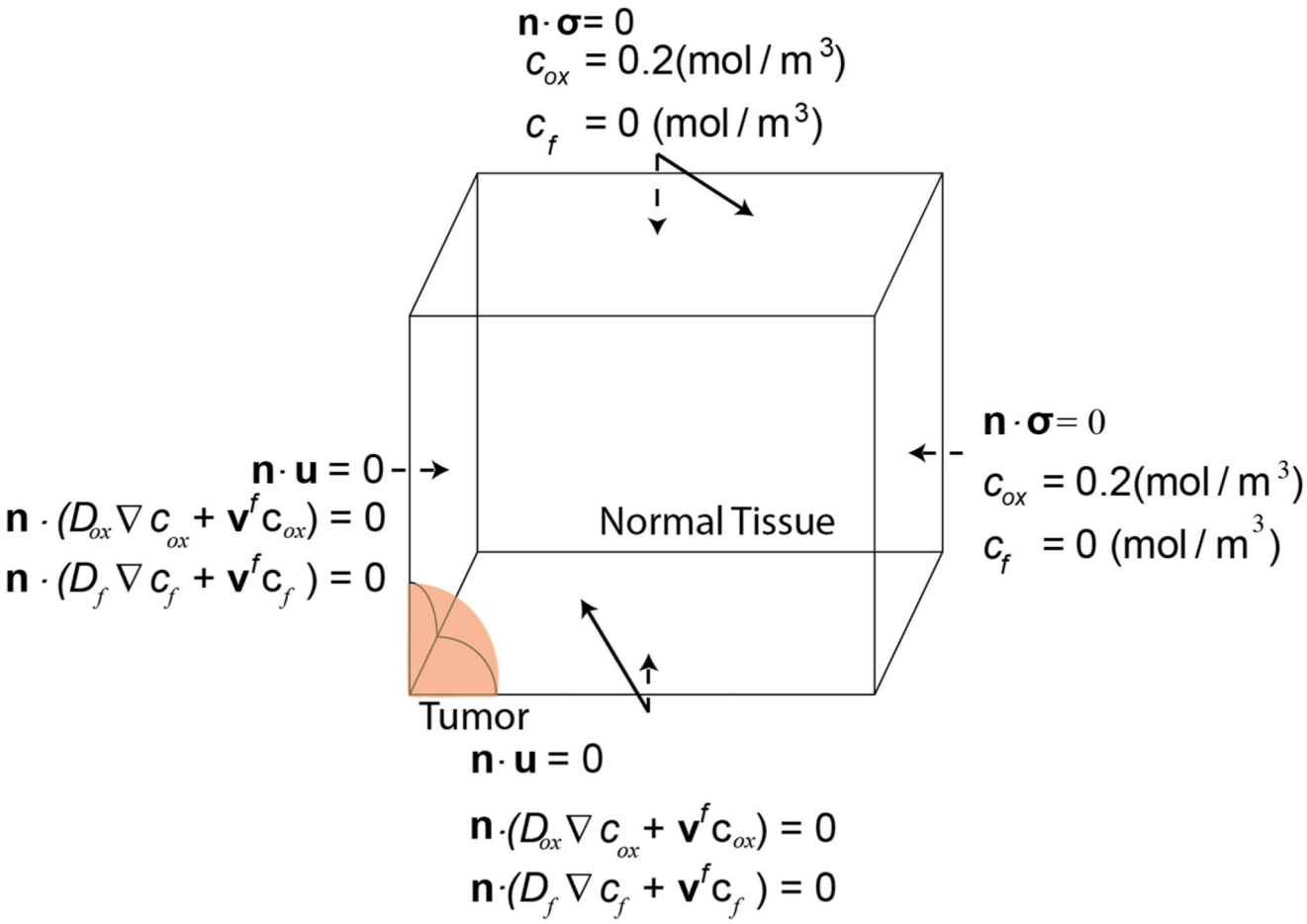

Fig. 1.
Geometry of the computational domain and boundary conditions employed.

Europe PMC Funders Author Manuscripts

Europe PMC Funders Author Manuscripts

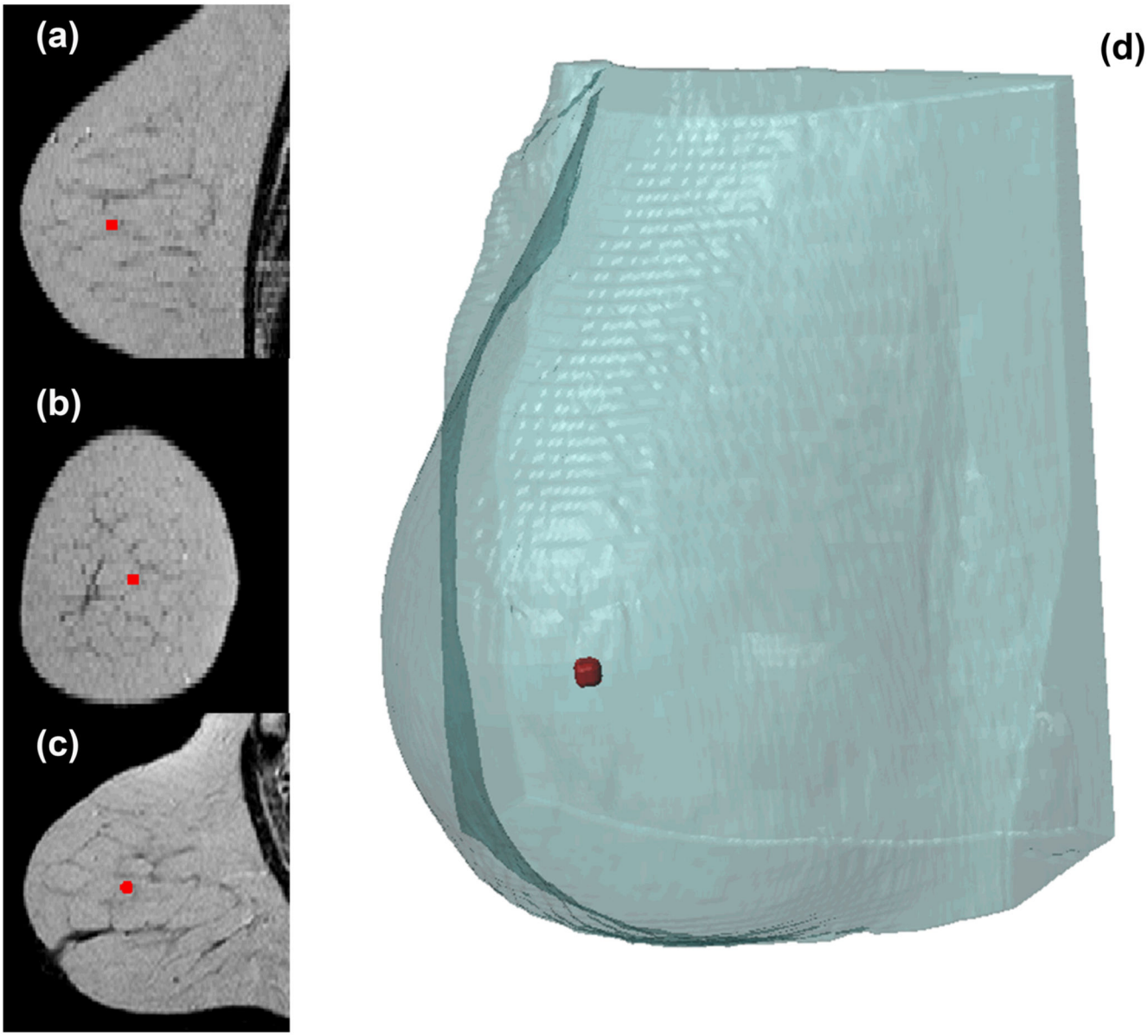

Fig. 2.

Sagittal **(a)**, coronal **(b)**, and axial **(c)** views of the acquired breast MR images. **(d)** Three-dimensional representation of the extracted mesh. The red colored region represents the position of the initial tumor seed.

Europe PMC Funders Author Manuscripts

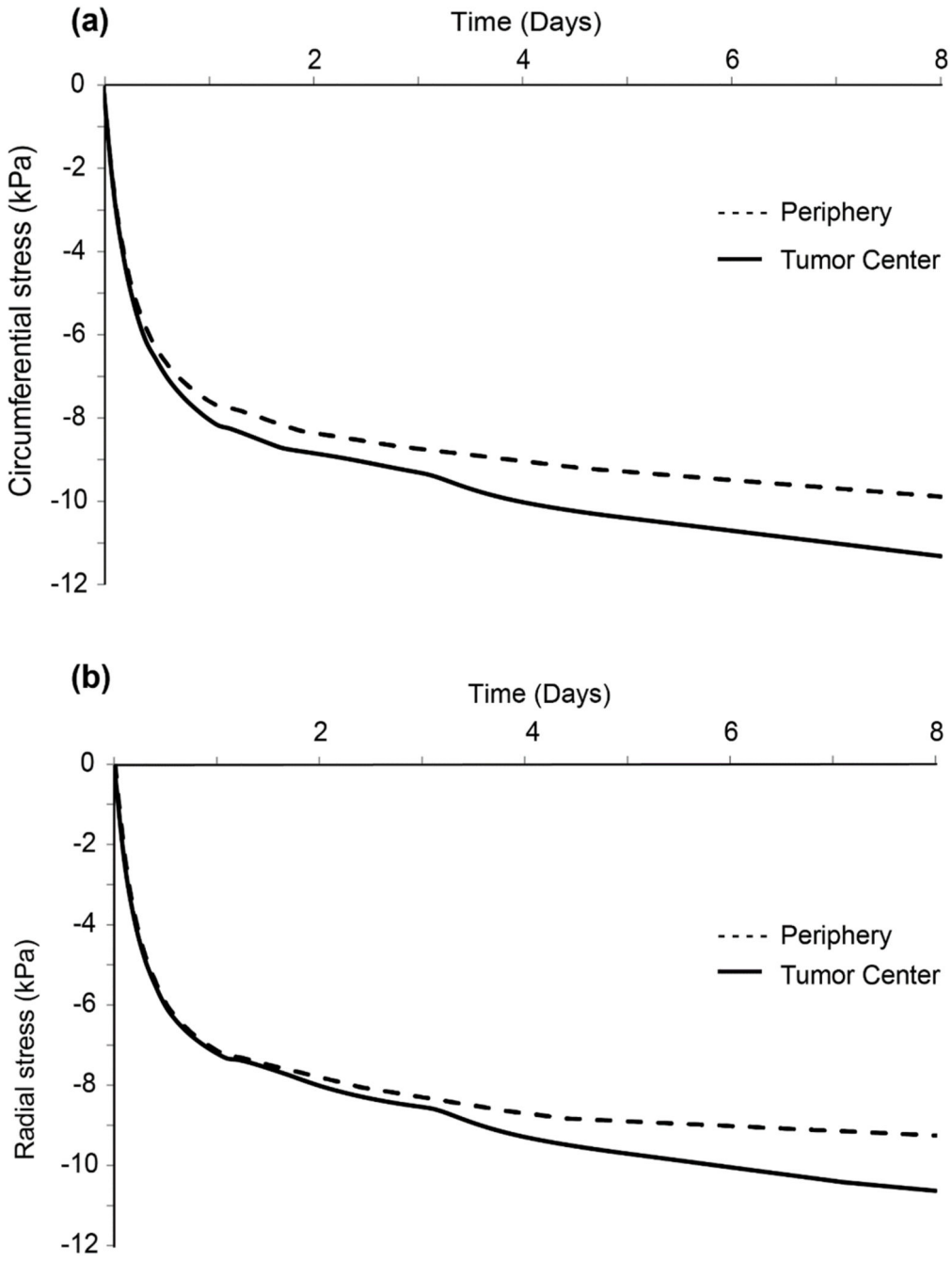

Fig. 3.

Circumferential and radial solid stress profile at the center and the periphery of the tumor. Stresses are higher in the center of the tumor compared to the periphery.

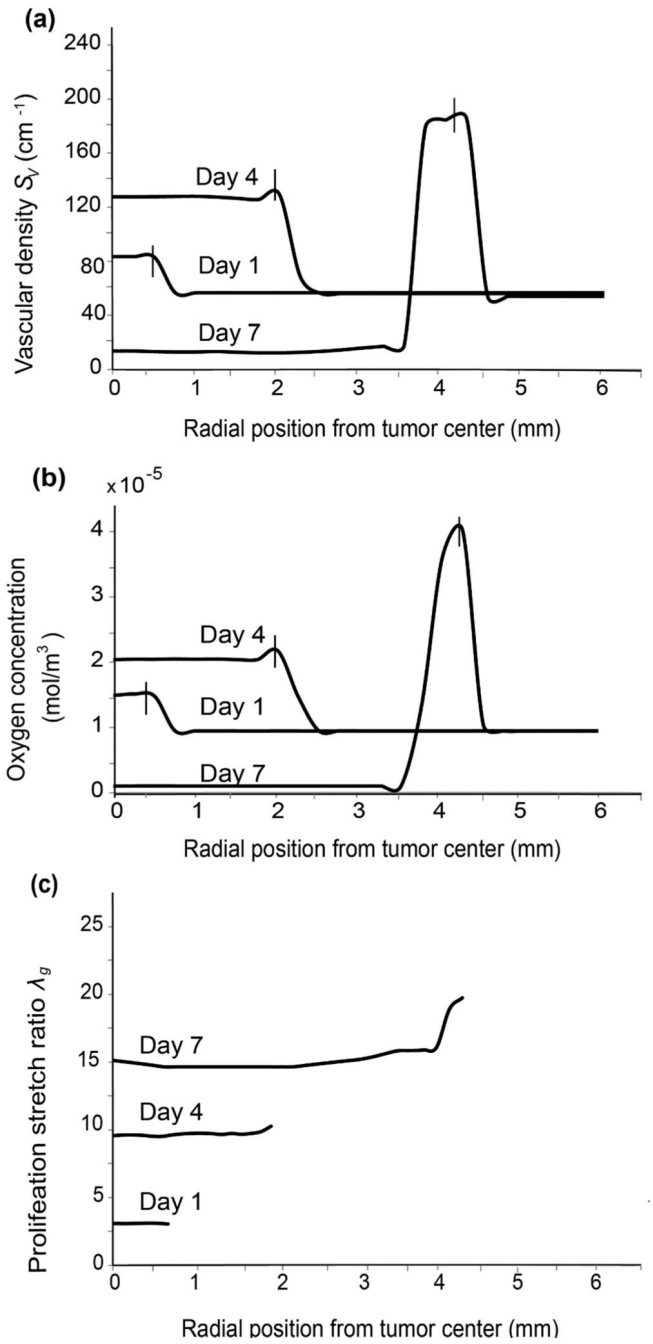

Fig. 4.

Effect of solid stress on vascular density, tumor oxygenation and cancer cell proliferation. **(a)** Spatial distribution of vascular density at different time instances (days). Intratumoral vascular density increases until Day 4 and then decreases following vessel collapse. It is also higher at the periphery than the tumor interior and constant in the healthy tissue away from the interface. After vessel collapse, vascular density is lower in the tumor interior than the surrounding healthy tissue (Day 7). **(b)** The spatial distribution of oxygen concentration at different time instances follows the same profile as vascular density. Vertical line segments

in **(a)**, **(b)** denote the position of the tumor-host tissue interface at the given time instance. **(c)** Spatial distribution of proliferation stretch during tumor growth. Larger oxygen concentrations at the tumor periphery eventually lead to higher values of cell proliferation than in the interior.

Europe PMC Funders Author Manuscripts

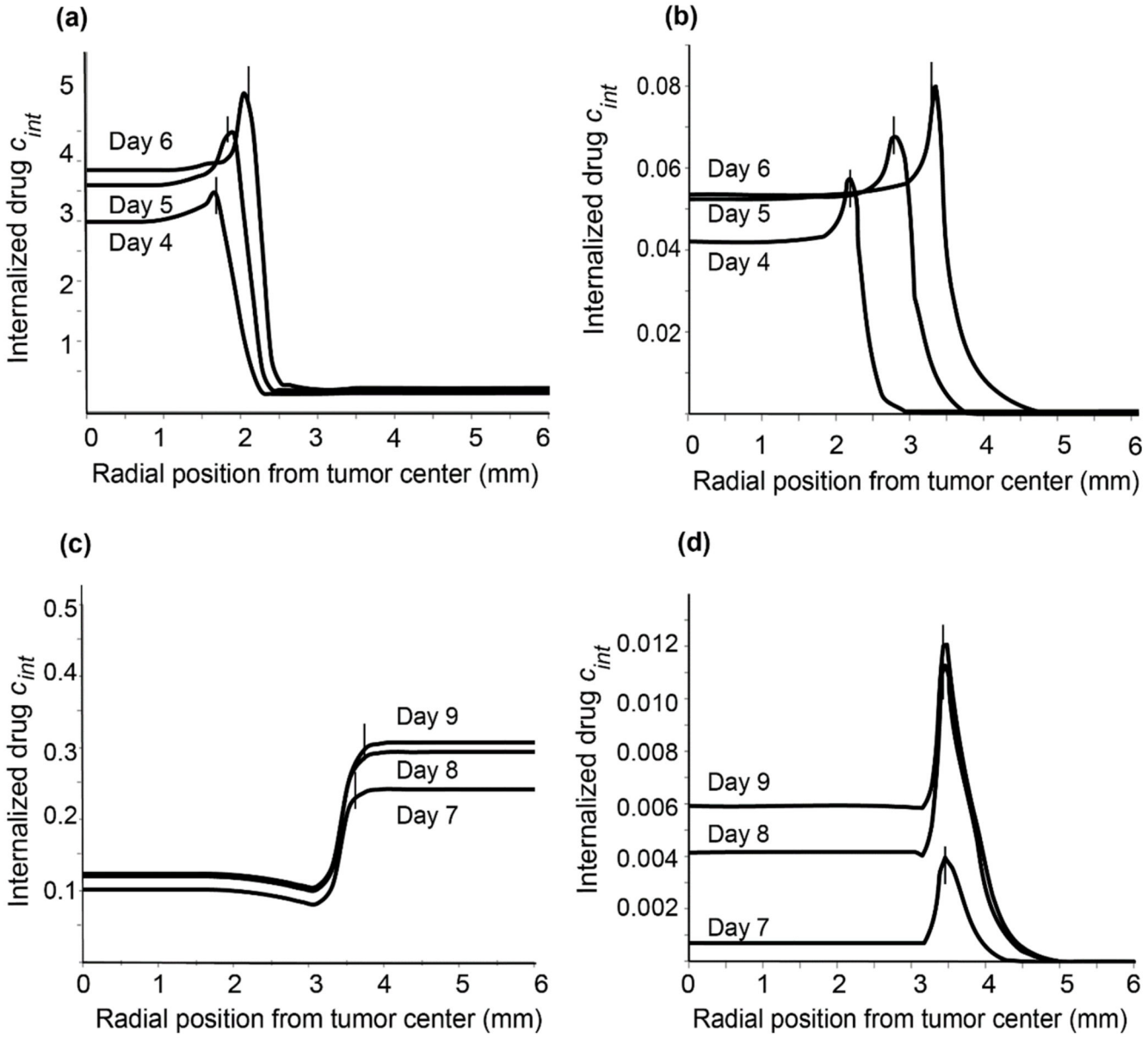

Fig. 5.

Intratumoral distribution of internalized drug concentration when the drug is administered before vessel collapse: **(a)** chemotherapy alone; **(b)** nanoparticle delivery system. Intratumoral distribution of internalized drug concentration when the drug is administered after vessel collapse: **(c)** chemotherapy alone; **(d)** nanoparticle delivery system. All concentrations have been rendered dimensionless after division with the initial vascular concentration. Vertical line segments in all panels denote the position of the tumor-host tissue interface at the given time instance.

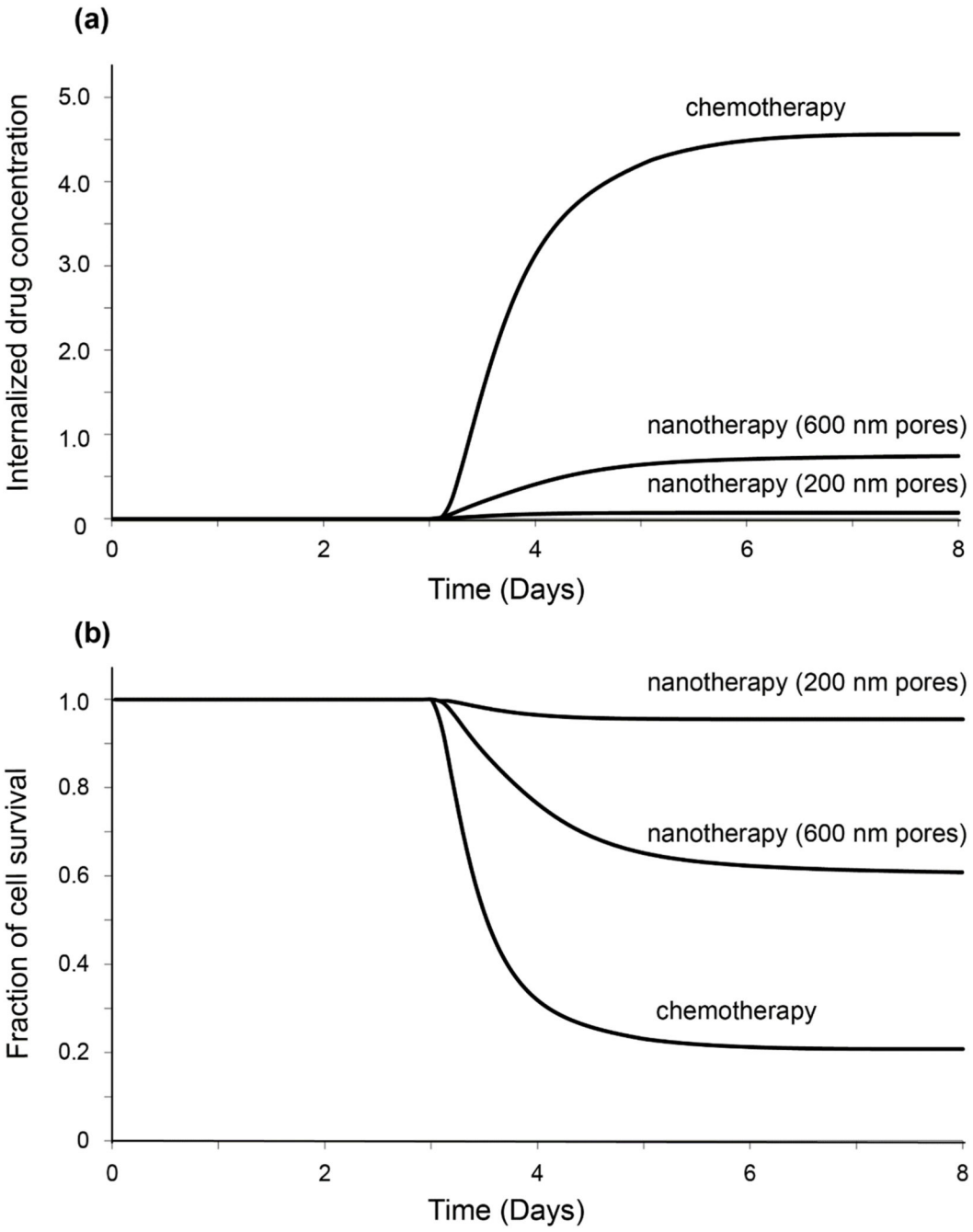

Fig. 6.

(a) Internalized drug concentration, administered prior to vessel collapse, as function of time for the two different treatments and for different pore sizes, namely, 200 nm and 600 nm. **(b)** Fraction of cell survival for the three cases considered in **(a)**.

Europe PMC Funders Author Manuscripts

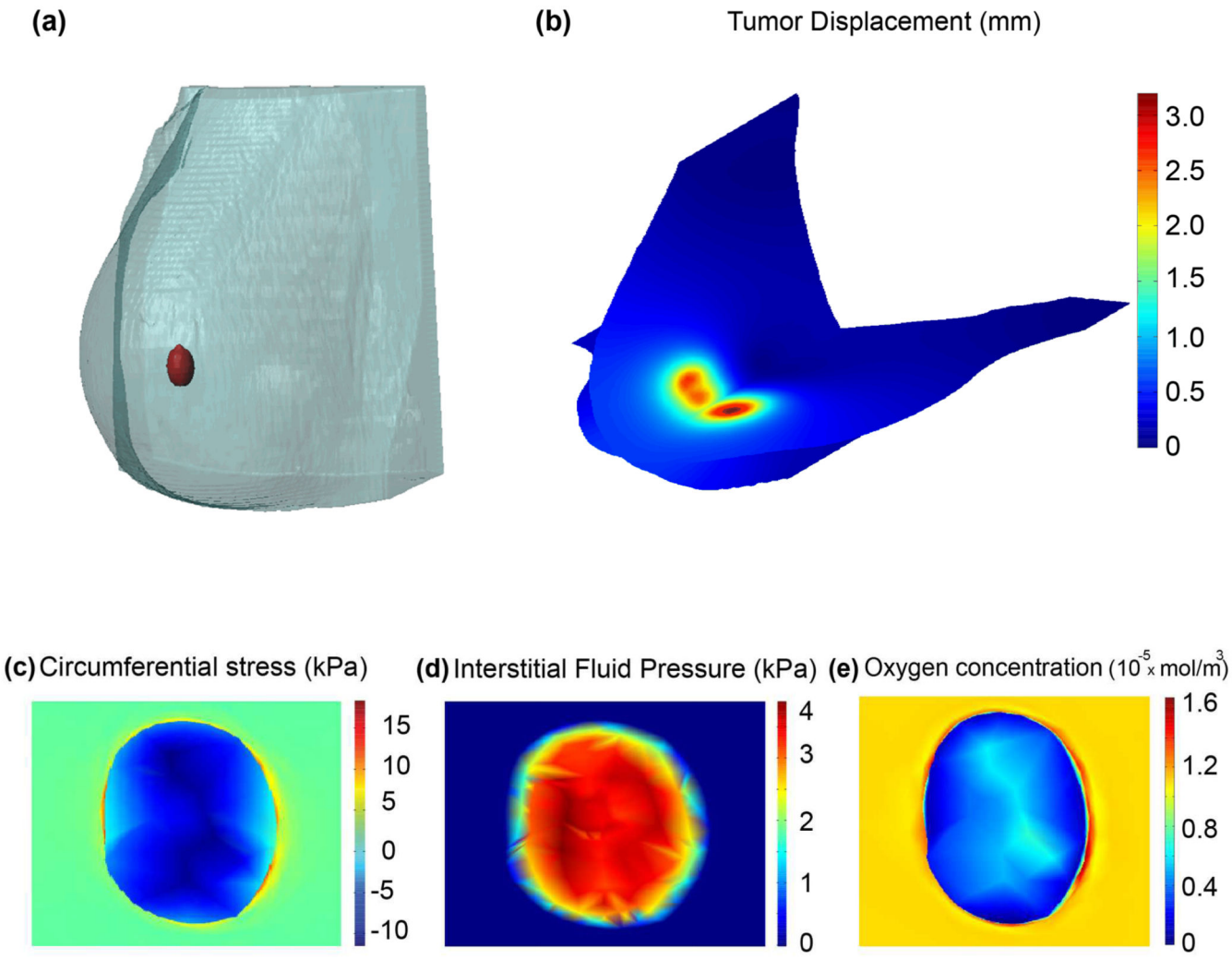

Fig. 7.

(a) Three-dimensional representation of the computational domain showing the final breast tumor size. **(b)** Total displacements map with higher tumor displacements observed in the anterior and cranio-caudal directions of the breast. **(c)** Solid stress is compressive in the interior and tensile at the periphery of the tumor. **(d)** Interstitial fluid pressure is higher at the center of tumor and drops to normal values at the periphery. **(e)** Solid stress results in lower oxygen levels at the interior of the tumor.

Table 1

Parameter values used in the model

Parameter	Description	Value	Reference
μ	shear modulus	5.00 kPa for host tissue; 10.40 kPa for tumor	(Netti et al. 2000; Samani et al. 2007; Eder et al. 2014)
k	bulk modulus	6.67 kPa for host tissue; 10.40×10^{7} kPa for tumor	(Netti et al. 2000; Samani et al. 2007; Eder et al. 2014)
k_{th}	hydraulic conductivity	1×10^{-12} m^2·Pa^{-1}·day^{-1}	(Netti et al. 2000)
β	growth stress dependence	0.000025 Pa^{-1}	(Voutouri et al. 2014)
C_{iox}	initial oxygen concentration	0.2 mol·m^{-3}	(Casciari et al. 1992a)
D_{ox}	oxygen diffusion coefficient	1.55×10^{-4}m^2·day^{-1}	(Kim et al. 2011)
A_{ox}	oxygen uptake	2,200 mol·m^{-3}·day^{-1}	(Casciari et al. 1992a; Kim et al. 2011)
k_{ox}	oxygen uptake	0.00464 mol·$^{-3}$	(Casciari et al. 1992a; Kim et al. 2011)
k_1	growth rate parameter	6,000 day^{-1}	---
k_2	growth rate parameter	0.0083 mol·m^{-3}	(Casciari et al. 1992a)
c_e	receptor concentration	0.01 mol·m^{-3}	(Mok et al. 2009; Schmidt and Wittrup 2009)
Φ	volume fraction of tumor accessible to drug	0.3 for 1 nm drug; 0.06 for 50 nm drug	(Mok et al. 2009; Schmidt and Wittrup 2009)
k_{on}	binding rate	1.296×10^{6} m^3·mol^{-1}·day^{-1}	(Mok et al. 2009; Schmidt and Wittrup 2009)
k_{off}	dissociation rate	691.2 day^{-1}	(Mok et al. 2009; Schmidt and Wittrup 2009)
k_{int}	internalization rate	3.7 day^{-1}	(Mok et al. 2009; Schmidt and Wittrup 2009)
k_{el}	chemotherapy release rate	0.181 day^{-1}	(Wong et al. 2011)
a	chemotherapy molecules contained in nanocarrier	10^4	(Dawidczyk et al. 2014)
D_f	drug diffusion coefficient	8.64×10^{-6} m^2·day^{-1} for 1 nm drug; 8.64×10^{-8}m^2·day^{-1} for 50 nm drug	(Pluen et al. 2001)
ω	cell survival constant	0.6603 m^3/mol	(Eikenberry 2009)
kd	blood circulation decay	0.417 day^{-1}	(Chauhan et al. 2012)